Chemical Science

ROYAL SOCIETY OF CHEMISTRY

EDGE ARTICLE

View Article Online
View Journal | View Issue

Cite this: *Chem. Sci.*, 2021, **12**, 12977

All publication charges for this article have been paid for by the Royal Society of Chemistry

Received 7th June 2021
Accepted 1st September 2021

DOI: 10.1039/d1sc03069h

rsc.li/chemical-science

A ratiometric photoelectrochemical microsensor based on a small-molecule organic semiconductor for reliable *in vivo* analysis†

Yunhui Xiang,[a] Yao Kong,[b] Wenqi Feng,[a] Xiaoxue Ye*[b] and Zhihong Liu *[a]

Photoelectrochemical (PEC) sensing has been developing quickly in recent years, while its *in vivo* application is still in the infancy. The complexity of biological environments poses a high challenge to the specificity and reliability of PEC sensing. We herein proposed the concept of small-molecule organic semiconductor (SMOS)-based ratiometric PEC sensing making use of the structural flexibility as well as readily tunable energy band of SMOS. Xanthene skeleton-based **CyOH** was prepared as a photoactive molecule, and its absorption band and corresponding PEC output can be modulated by an intramolecular charge transfer process. As such, the target mediated shift of absorption offered the opportunity to construct a ratiometric PEC sensor. A proof-of-concept probe **CyOThiols** was synthesized and assembled on a Ti wire electrode (TiWE) to prepare a highly selective microsensor for thiols. Under two monochromatic laser excitation (808 nm and 750 nm), **CyOThiols**/TiWE offered a ratiometric signal (j_{808}/j_{750}), which exhibited pronounced capacity to offset the disturbance of environmental factors, guaranteeing its reliability for application *in vivo*. The ratiometric PEC sensor achieved the observation of bio-thiol release induced by cytotoxic edema and fluctuations of thiols in drug-induced epilepsy in living rat brains.

Introduction

Abnormal concentration fluctuations of neurotransmitters, neuromodulators and other signalling molecules are closely associated with many brain-related physiological and pathological events.[1] Thus, monitoring the dynamics of extracellular neurochemicals *in vivo* can provide direct insight into the molecular basis of brain function. There has been ever increasing interest in the development of reliable and effective analytical protocols for *in situ* monitoring of neurochemicals. *In vivo* electrochemical (EC) analysis is a promising tool for such tasks due to the merits of high spatial–temporal resolution and favorable sensitivity. A variety of EC microsensors have been rationally designed in the last few decades for monitoring extracellular neurochemicals employing their inherent physicochemical properties in the brain.[2]

As an important new branch of EC analysis, photoelectrochemical (PEC) assay has undergone rapid development in recent years and shown its prospect for *in vivo* research.[3] Instead of exerting an external bias to trigger an electrochemical readout as traditional EC assays do, a local potential at the photoelectrode surface is generated by applying light excitation to photoactive materials in PEC sensing, which provides higher biocompatibility and a reduced background signal as compared to conventional EC assays.[3a,4] Nonetheless, its application for *in vivo* analysis has rarely been reported, since it is facing two major challenges, namely specificity and reliability in complex biological environments.[5] To address the concern of specificity, we recently proposed a fluorescence resonance energy transfer (FRET) modulated PEC sensing strategy.[6] The introduction of chemical recognition towards a target and modulation of the electrochemical readout by an optical process enabled the specific detection of diverse analytes (both electroactive and electrochemically non-active) in live animals. So far, however, there has been no solution to ensure the reliability and accuracy of PEC sensing *in vivo*. Because of the high sensitivity, the photocurrent response is prone to be impacted by instrumental or environmental factors. For example, the co-existing reductive substances like ascorbic acid (AA), dopamine (DA), 5-hydroxytryptophane (5-HT) and so forth in the physiological environment are likely to lead to false positive or false negative results.[3a] This is decided by the principle of PEC sensing, which relies on a hole (or electron) trapping agent for signal outputting.

As well documented, ratiometric signal output has strong anti-interference capability and presents much higher reliability in complex environments.[7] The ratiometric signal has

[a]*College of Chemistry and Molecular Sciences, Wuhan University, Wuhan 430072, China. E-mail: zhhliu@whu.edu.cn*

[b]*College of Chemistry and Chemical Engineering, Hubei University, Wuhan 430062, China. E-mail: yexxchem@hubu.edu.cn*

† Electronic supplementary information (ESI) available: Text, figures and tables depicting synthetic procedures, detailed experimental procedures, and characterisation data. See DOI: 10.1039/d1sc03069h

been widely employed in optical probes but is seldomly seen in PEC sensing.[8] Very few ratiometric PEC sensors were fabricated by using two photoactive materials or two photoelectrodes, which, however, still remains uncertain because it is hard to offset the systematic error between the two electrodes or two photoactive materials.[9] Besides, the rather complicated photoelectrode modification process is unfavourable for the reproducibility of assay. Hence, it would be ideal to construct a ratiometric PEC sensor using a single photoactive material with a single photoelectrode. Unfortunately, the energy level and chemical structure of photoactive materials (mostly inorganic semiconductors) are hard to tune by the target recognition process, which makes it nearly impossible to output two self-calibrated signals before and after the response to targets.[10]

A small-molecule organic semiconductor (SMOS) is another kind of photoactive material with wide application in photovoltaic fields.[11] As a structurally flexible small molecule, it is not hard to modulate the HOMO–LUMO energy-level difference through regulating the electron-pushing (or pulling) capacity of an electron donor (or acceptor) or the length of the conjugate chain of the molecule.[12] Such a readily tunable band gap gives us a hint that we might be able to adjust the energy-level difference of a SMOS upon its response towards a specific target (typically a chemical reaction) *via* a rational structural design. The change of the energy-level difference will possibly cause the variation of its optical absorption, thus offering the opportunity to generate two PEC output signals at two optical channels.[12b] Inspired by this, we herein put forward the concept of a SMOS-based ratiometric PEC sensor. To facilitate its use in the living body, which requires a large penetration depth of light, a SMOS based on the xanthene skeleton by introducing 1-propyne-2-methyl-benz[*c*,*d*]indolium salt (named **CyOH**) absorbing in the NIR region was prepared as the photoactive molecule. By substituting the hydrogen of –OH with different electron-donating or withdrawing groups, the structure–activity relationship of SMOSs was looked into. Thereafter, as a proof of concept, we constructed a wavelength-resolved ratiometric PEC microsensor (named **CyOThiols**) through the incorporation of a recognition group for thiols at the –OH position (Scheme 1). The NIR-light driven PEC sensor was utilized to monitor the levels of thiols in live rat brains. The fluctuations of thiols in the process of cytotoxic edema and drug-induced epilepsy in rat brains were evaluated. The SMOS here acted as both the photoactive material and the carrier of recognition units. To the best of our knowledge, this is the first SMOS-based ratiometric PEC sensor, which not only achieved self-calibrated measurement but also simplified the configuration of the photoelectrode, significantly improving the reliability of *in vivo* sensing.

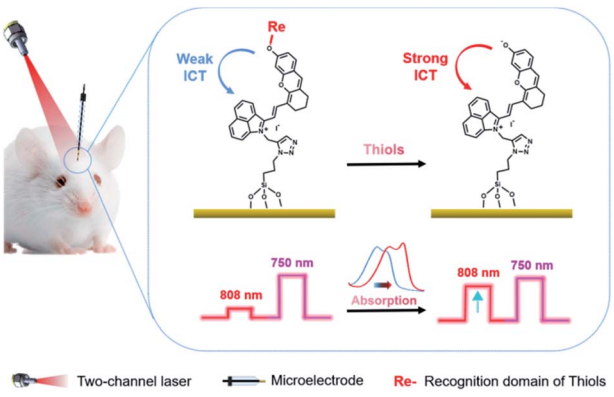

Scheme 1 Design principle of the ratiometric PEC microsensor based on **CyOH**.

Results and discussion

Design and photophysical properties of SMOSs

Typically, an electron donor (D)–π–electron acceptor (A) type dipolar structure is beneficial to the intramolecular charge transfer (ICT) process so as to red-shift the absorption band of an organic dye. Herein, 1-propyne-2-methyl-benz[*c*,*d*]indolium salt was selected as an electron acceptor, in which benz[*c*,*d*]indolium salt acts as a strong electron-pulling end. 6-Hydroxyl-2,3-dihydro-1*H*-xanthene-4-carbaldehyde with a large conjugated plane was used as the conjugate skeleton. The hydroxyl group at the 6-position was designed as the electron-pushing end and utilized to regulate the optical absorption and the photoelectrochemical properties, since, as known, the electron-pushing/pulling effect of –OH can be flexibly switched between the modification and release of this group.[12b] The two motifs, *i.e.*, 1-propyne-2-methyl-benz[*c*,*d*]indolium salt and 6-hydroxyl-2,3-dihydro-1*H*-xanthene-4-carbaldehyde, were connected through a Knoevenagel reaction to prepare **CyOH** with a D–π–A structure (Scheme S1c†).[12a] The terminal acetylene group was designed as a reaction site for the immobilization of the molecules onto the electrode surface *via* a click reaction. To investigate the structure–activity relationship of SMOSs, we incorporated two representative substituents (methyl and carbethoxy groups) into the hydroxyl position of **CyOH**, resulting in **CyOMe** and **CyOAc**, respectively (Scheme S1†). All the synthesized organic compounds were confirmed by ^{1}H NMR and HRMS (Fig. S1–S6†).

As shown in Fig. 1a, **CyOH** (760 nm) and **CyOMe** (753 nm) had similar maximum absorption wavelengths, while **CyOAc** showed the maximum absorption at 734 nm. The obvious blue shift of the absorption band of **CyOAc** can be attributed to the strong electron-pulling effect of the carbethoxy group, which effectively weakened the electron-donating ability of the oxygen

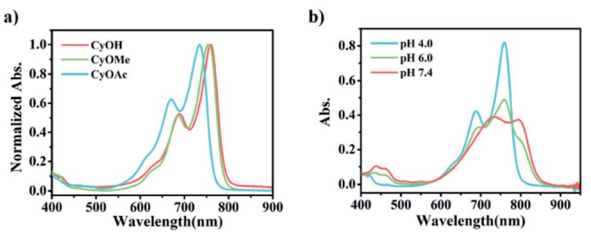

Fig. 1 Absorption spectra of (a) **CyOH**, **CyOMe** and **CyOAc** in PBS buffer at pH 4.0 and (b) **CyOH** at pH 4.0, 6.0 and 7.4, respectively (PBS/MeCN = 6 : 4).

atom and thus reduced the ICT effect.[12b] To further assess whether the modification/release of the hydroxyl group could alter the ICT effect, the absorption spectra of **CyOH** were recorded in aqueous buffers with different pH values, where the molecule exists in a protonated or deprotonated form (Scheme S2†). As the pK_a of **CyOH** was calculated to be 6.2 according to the Henderson–Hasselbalch-type mass action equation,[13] we selected pH 4.0, 6.0 and 7.4 for tests. As shown in Fig. 1b, the protonated form exhibited a maximum absorption at 753 nm (pH 4.0), and there was a 42 nm red shift of absorption at pH 7.4 (the peak at 795 nm). This is explained by the strong electron-donating ability of the deprotonated hydroxyl group, which enhanced the ICT efficiency. Besides, the absorbance of **CyOH** at 808 nm (the wavelength of a commonly used commercial laser) kept constant in the physiological pH range (Fig. S7†). The above results suggested the possibility to make **CyOH**-based sensors by modifying a specific recognition group on –OH, given that the modification weakens the electron-donating ability of the oxygen atom and thus reduces the ICT effect. Once **CyORe** (Re refers to the recognition domain of the target) specifically reacted with the target to give **CyOH**, which then further deprotonated at physiological pH, the ICT effect would be remarkably strengthened, and therefore an obvious red shift of the absorption wavelength after the target recognition can be acquired. Therefore, an increased photocurrent under longer-wavelength (808 nm) excitation relative to that under shorter-wavelength (750 nm, set as a built-in reference) excitation after the recognition reaction could be expected. By employing these two distinguished excitation channels, the construction of ratiometric PEC sensors based on a SMOS would become possible.

Theoretical calculations

To have a better understanding of the structure–activity relationship of **CyOH** and its derivatives, density functional theory (DFT) calculations at the B3LYP/6-31G(d,p) level with Grimme's dispersion correction (D3-BJ) in water (PCM solvent model) using the Gaussian 16 program were performed. Orbital composition analysis was performed by using Multiwfn software.[14] Fig. 2 and S8† show the representative optimized structures and molecular orbital plots (LUMO and HOMO) of the substances including **CyO$^-$**, **CyOH**, **CyOMe** and **CyOAc**. The HOMO and LUMO were all mainly located on the π-conjugated system of **CyO$^-$**, **CyOH**, **CyOMe** and **CyOAc**. However, the contributions of O-linked functional groups were different, which were calculated by Mulliken partition and the obtained results are listed in Table S1.† The basic characteristics of a molecule with the ICT effect is that the HOMO is distributed at the electron donor (D) end, and the LUMO is distributed at the electron acceptor (A) end. Therefore, the contribution of substituents to D will lead to the enhancement of the ICT effect, resulting in the increase of electron mobilities in the molecular conjugate system and a narrowed HOMO–LUMO gap. On the macro view, it will eventually cause a redshift in the absorption wavelength. It is shown that the contribution to the HOMO and LUMO increased with the electron-donating ability

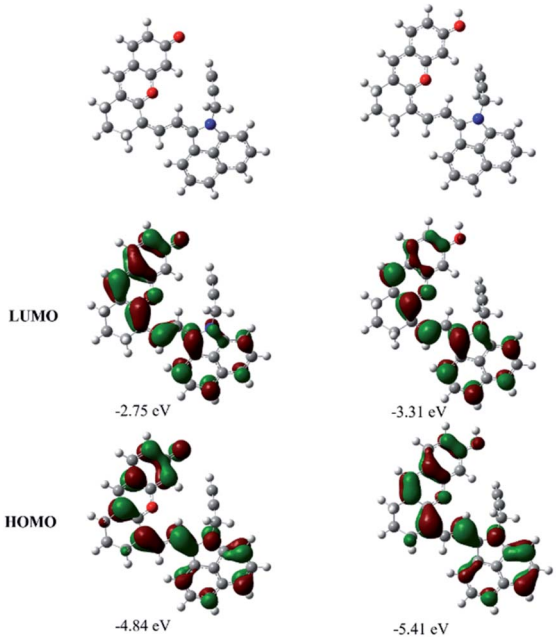

Fig. 2 DFT optimized structures and molecular orbital plots (LUMO and HOMO) of **CyO$^-$** (left column) and **CyOH** (right column) in water based on the optimized ground-state geometry (S_0). In the ball-and-stick representation, carbon, nitrogen, and oxygen atoms are shown in grey, blue, and red, respectively.

strengthening, which is consistent with the basic characteristics of the ICT effect. Since the transition of $S_0 \rightarrow S_1$ was mainly contributed by the electron transition from the HOMO to the LUMO, the difference of the contribution (HOMO–LUMO) reflected the level of ICT. That is, the ICT effect was enhanced by the electron-donating ability, resulting in the strongest ICT effect of **CyO$^-$** and the weakest ICT effect of **CyOAc**. Comparing the HOMO–LUMO gaps among **CyO$^-$**, **CyOH**, **CyOMe** and **CyOAc** (Table S2†), it is also found that the gap decreased with the electron-donating ability strengthening. The absorption spectra of these compounds can be explained by the gap variation: the lower the gap, the longer the absorption. Additionally, the variation trend of experimental spectral results was basically in agreement with the theoretical calculations. In a word, DFT calculations proved that the structure–activity relationship of **CyOH** and its derivatives exhibited the typical characteristics of the ICT effect, *i.e.* the intensity of ICT decided the shift of the absorption band, which is the physical basis for constructing a ratiometric PEC sensor.

Photoelectrochemical properties of SMOSs

A piece of titanium wire with a diameter of 100 μm was used as the working electrode. To guarantee the stability and reproducibility of modified electrodes, SMOSs were chemically bonded to the surface of the electrode *via* a process shown in Scheme 2. Briefly, 3-(azidopropyl)triethoxysilane was connected to the hydroxylated Ti wire through a silicon–oxygen bond, and the as-obtained wire was denoted as TiWE. Energy dispersive spectroscopy (EDS) analysis showed increased C and Si contents

after this modification step, indicating the successful preparation of TiWE (Fig. S9†). *In situ* Fourier transform infrared spectroscopy (IS-FTIR) (Fig. S10†) also revealed that there were plenty of azido groups (2105 cm^{-1}) on the surface of TiWE. 1 mm length of TiWE was reserved for the subsequent loading of SMOSs, while the remaining part was encapsulated in a capillary tube (Fig. S11a†). Then, **CyOR** (R = –H, –Me, –Ac) were separately fixed on the surface of the TiWE electrodes by a Cu-catalyzed click reaction between the terminal acetylene group of **CyOR** and the azido group of the electrode surface. The scanning electron microscope (SEM) image (Fig. S11b and c†) exhibited a rough surface of TiWE, which is beneficial to increase the effective area for **CyOR** immobilization and in favourable for interfacial reactions.[10,15]

The effect of different substitution groups at hydroxyl on the photoelectrochemical properties of SMOSs was investigated. As shown in Fig. 3a, all three **CyOR** molecules produced obvious photocurrent signals under both 808 nm and 750 nm excitation. Further observations of the relationship between photocurrent intensities and the concentration of ascorbic acid (AA), which is a commonly used electron provider for anodic photocurrent measurements, indicated that the photocurrent generation had an obvious dependence on the amount of reductive reactant such as AA (Fig. S12†). According to a previously reported photoelectrochemical mechanism for SMOSs like toluidine blue and methylene blue,[4,16] we briefly interpreted the photoelectrochemical reaction of **CyOR** as shown below, which consists of three consecutive steps: the organic molecule S transformed into its corresponding excited state upon light excitation (eqn (1)), and the reductive reactant (AA) could reduce the excited state to $(S^*)_{red}$ (eqn (2)), which may transfer electrons to the electrodes and generate anodic photocurrent (eqn (3)).

$$S \xrightarrow{h\nu} S^* \quad (1)$$

$$S^* + AA \rightarrow (S^*)_{red} + (AA)_{ox} \quad (2)$$

$$(S^*)_{red} \rightarrow S + e^- \quad (3)$$

Since CyO^- (the deprotonated form of **CyOH**) had maximal absorption at around 800 nm, its anodic photocurrent intensity was higher than the other two molecules under 808 nm excitation, whereas its photocurrent intensity was lower than the other two under 750 nm excitation. Notably, the ratiometric signal (j_{808}/j_{750}) of CyO^-/TiWE was 3.3 times larger than that of **CyOMe**/TiWE and 4.5 times larger than that of **CyOAc**/TiWE (Fig. 3b), further implying the rationality of making ratiometric PEC sensors by modifying certain recognition groups on –OH, taking the photocurrent signal under 750 nm excitation as a built-in reference.

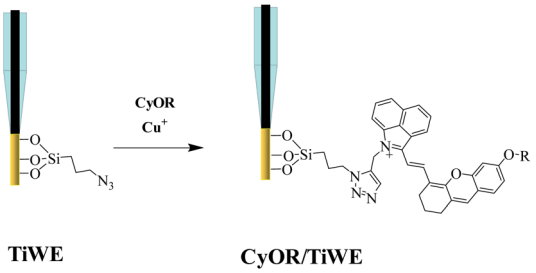

Scheme 2 Assembly process of **CyOR** on TiWE. R = –H, –Me and –Ac.

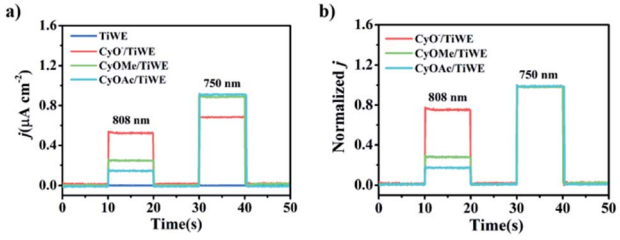

Fig. 3 (a) Photocurrent intensities of bare TiWE, CyO^-/TiWE, **CyOMe**/TiWE and **CyOAc**/TiWE and (b) normalized photocurrent intensities of CyO^-/TiWE, **CyOMe**/TiWE and **CyOAc**/TiWE in 0.1 M aCSF containing 250 μM AA excited with 808 nm and 750 nm lasers, respectively. Intensities under 750 nm excitation in (b) were set as a built-in reference.

Response performance of the ratiometric PEC microsensor for thiols

Thiols are thought to play critical roles in various physiological and pathological processes. An abnormal level of thiols in organisms indicates a variety of diseases such as organ damage, neurodegenerative diseases, and slower growth.[17] Thus, it is of high interest to monitor total biological thiols in the body. A chemosensor for thiols, **CyOThiols**, was synthesized by incorporating a recognition domain of thiols (2,4-dinitrobenzenesulfonyl chloride) on the hydroxyl group of **CyOH** (Scheme S3†). The structure of **CyOThiols** was confirmed by ^1H NMR and HRMS (Fig. S13†). Optical absorption measurements were firstly conducted to verify the response of **CyOThiols** towards thiols, in which we used cysteine (Cys) to represent thiols since thiols equilibrate with each other in biosystems.[17c] As demonstrated in Fig. 4a, **CyOThiols** itself exhibited a strong absorption band at 734 nm, which was similar to that of **CyOAc**. After reacting with Cys, the absorption peak red-shifted to

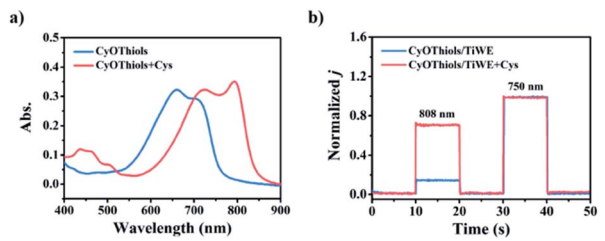

Fig. 4 (a) Absorption spectra of 6 μM **CyOThiols** in pH 7.4 PBS/MeCN (6 : 4) before and after reacting with 500 μM Cys for 5 min. (b) Normalized photocurrent intensities of **CyOThiols**/TiWE in 0.1 M PBS containing 250 μM AA driven by 808 nm and 750 nm lasers before and after reacting with 500 μM of Cys for 5 min.

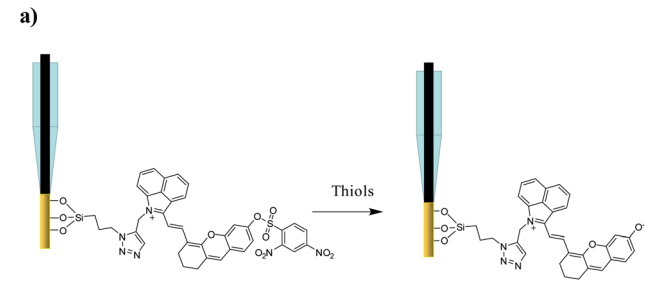

Scheme 3 Recognition reaction of Thiols by **CyOThiols**/TiWE.

795 nm, which was the result of Cys mediated structural transformation from **CyOThiols** into **CyO**$^-$ (Scheme 3). The reaction was quick and completed in only 2 minutes, and the absorption of the product was stable (Fig. S14†).

To fabricate a ratiometric PEC microsensor for thiols, **CyOThiols** was immobilized on TiWE *via* the above-mentioned click reaction. Correspondingly, an increased photocurrent signal under 808 nm excitation was obtained in the presence of Cys, when normalized to the photocurrent obtained under 750 nm excitation (Fig. 4b). Due to the involvement of interface mass transfer, the response time of **CyOThiols**/TiWE to Cys was longish but the reaction still completed within 4 minutes (Fig. S15†). To study the selectivity of the PEC microsensor, various potential interfering species were investigated in parallel under the same conditions. As shown in Fig. S16,† after incubating with those interfering species alone, no obvious photocurrent response was detected, and the co-incubation of the species and Cys didn't cause a significant change of the photocurrent response of Cys, indicating a pronounced specificity of **CyOThiols**/TiWE towards thiols over the other species. A good linear relationship was established between the ratiometric signal (j_{808}/j_{750}, denoted as r in Fig. S17†) and the logarithm of Cys concentration, log(c) in the ranges of 2.0 to 100 μM: $r = 0.194 \log(c) + 0.018$ ($R^2 = 0.993$) and 100 to 1000 μM: $r = 0.441 \log(c) - 0.475$ ($R^2 = 0.996$), and the limit of detection was calculated to be 0.65 μM, which laid down the foundation for the quantitative detection of the target.

The stability, reproducibility and biocompatibility of the microsensor **CyOThiols**/TiWE were then investigated. Under continuous irradiation with 808 nm and 750 nm lasers for 380 s, the photocurrent signal of **CyOThiols**/TiWE kept unchanged, which can be attributed to the good photostability of **CyOThiols** as well as the stable bonding of **CyOThiols** on the TiWE surface (Fig. S18†). In addition, the standard deviation for 12 microelectrodes tested in the same rat brain was <5.14%, indicating a good reproducibility of the as-prepared photoelectrode (Fig. S19†). Biocompatibility was assessed by propidium iodide and calcein-AM staining of cells incubated on a **CyOThiols** modified titanium sheet and the infrared thermal imaging of the photothermal effect caused by 750 nm and 808 nm laser irradiation. As illustrated by the fluorescence staining in Fig. S20,† the cells growing on the surface exhibited a very high viability. Meanwhile, the infrared thermal imaging showed that the local temperature of light spots on the rat skull only increased by less than 1 °C after 750 nm and 808 nm laser irradiation for 10 s (Fig. S21†). These results suggested a good biocompatibility of the microsensor and the feasibility of using the microsensor for *in vivo* analysis.

Capacity of offsetting the environmental disturbance of the ratiometric PEC microsensor

The reliability of sensing strongly relies on the ability of the sensor to offset environmental disturbance to the detection signal, especially in highly complex samples like live bodies. For PEC sensing depending on the reductive reactant as the electron donor, the variation or inhomogeneous distribution of the reactant concentration may cause the distortion of the signal. Besides, the non-specific adsorption of biomolecules on the electrode surface or unidentical intensity/power of excitation light are also major issues challenging the reliability and accuracy of sensing.[18] Therefore, the anti-disturbance capacity of the ratiometric PEC sensor **CyOThiols**/TiWE was evaluated. Firstly, the impact of concentration of the reductive reactant (with AA as a representative) was examined. We tested three batches of samples containing 10, 70 and 500 μM Cys, respectively, all with varying amounts of AA (100–600 μM). As shown in Fig. S22a, c and e,† the absolute intensities of photocurrent were all greatly elevated with the increase of AA concentration. Since our subsequent *in vivo* analysis in the brain will employ intrinsic AA in the parenchyma, which is liable to fluctuate, the uncertainty of absolute photocurrent intensity at a single wavelength is inevitable. Thanks to the self-calibration of ratiometric measurement, the sensor offered a stable r (j_{808}/j_{750}) value with varying amounts of AA (Fig. S22b, d and f†). As shown in Table S3,† the recovery of Cys determined with the ratiometric mode was in the range of 90–110% in the presence of different concentrations of AA, indicating a good quantification capability of the sensor. Similarly, we also evaluated the influence of the non-specific adsorption of biomacromolecules using BSA as a representative molecule. As presented in Fig. S23a,† the change of BSA concentration had little effect on the ratiometric PEC signals, and the recoveries of Cys were between 91 and 108% for all groups. Fig. S23b† shows the photocurrent signals obtained at one photoelectrode excited for 16 cycles with 808 nm and 750 nm light in the cortex of a normal rat brain. As expected, although the absolute photocurrent intensity decreased by *ca.* 28% due to the non-specific adsorption of biomacromolecules on **CyOThiols**/TiWE, there was little variation in the ratiometric signal with a standard deviation of 4.32%. The unidentical intensity/power of excitation light can be caused by factors like the unfixed distance between the light source and the electrode, which is much likely to occur in practical operation. In our system, we used a coaxial optical fiber containing 750 nm and 808 nm beams to make sure the two light sources are located at a same distance (Fig. S24†). Then we tested the influence of the electrode-to-optical fiber distance on the PEC signal. As shown in Fig. S25a,† the distance clearly affected the PEC signals of both light channels, but there was negligible influence on the ratiometric signal at different distances (Fig. S25b†). All the above results and interpretations

have revealed the distinct advantage of ratiometric PEC signals over single-wavelength photocurrent output in terms of reliability.

In vivo monitoring of thiols in rat brains

Astrocytes providing structural, metabolic, and trophic support for neurons are dynamic cells with unique properties that enable them to respond to small changes in their environment.[19] Pathological changes in astrocytes may cause neurological disturbances such as ischemia, seizures, stroke, and spreading depolarization.[20] Astrocyte swelling is the leading cause of cerebral edema, and many studies have investigated the changes of ions and neurochemicals during astrocyte edema.[20b] Increasing evidence has indicated that astrocytes responded to edema status *via* releasing some other substances into the interstitial fluid.[19c,21] However, due to the limitation of the detection technique, the molecular mechanism of astrocyte swelling is still unclear. Hence, we are interested in exploring whether there are thiols released during cerebral edema caused by astrocyte swelling. We firstly investigated the changes of the thiol level in the event of cytotoxic edema in living rat brains. As shown in Fig. 5a, compared with the normal rat brain, an increased ratiometric PEC signal was recorded by **CyOThiols**/TiWE in the model of astrocyte swelling induced by the glutamate receptor agonist (*N*-methyl-D-aspartic acid, NMDA).[20b] To preclude the influence of the injection process, we conducted parallel experiments with artificial cerebrospinal fluid (aCSF) as the control. As shown in Fig. 5b, no obvious increase of the ratiometric PEC signal was recorded with the infusion of aCSF. Besides, our above selectivity assessment (Fig. S16†) has already excluded the influence of NMDA itself on the sensor. It thus can be concluded that the monitored response was caused by thiol release. To further explore the functions of cytotoxic edema in thiol efflux, different concentrations of NMDA (100, 300, 500, and 1000 μM, respectively) were injected into rat brains. As shown in Fig. S26† and 5c, in response to 300, 500, and 1000 μM NMDA, the ratiometric PEC signals (r) were increased to 1.17, 1.51 and 2.13 times higher than that of the control group, respectively. The results demonstrated a clear NMDA concentration-dependent thiol efflux.

Encouraged by the above findings, we set out to explore the possible mechanism involved in the thiol release in response to cytotoxic edema. A few earlier studies reported that cytotoxic edema can be efficiently inhibited by 4,4′-diisothiocyanatostilbene-2,2′-disulfonic acid (DIDS), through the inhibition of Cl^- flowing into the cell.[20b] Therefore, DIDS treatment could provide some important mechanistic information associated with the thiol release. As shown in Fig. 5d and e, no perceptible increase of the ratiometric PEC signal was found with the co-injection of 500 μM NMDA and 5 mM DIDS into the rat brain ($n = 3$), implying a completely diminished release of thiols accompanied by the inhibition of cytotoxic edema. For further validating thiol release induced by NMDA, we exploited NIR-II fluorescence imaging employing **CyOThiols** as a thiol-specific fluorescent probe (Fig. S27†). As shown in Fig. S28,† clear NMDA-driven fluorescence enhancement was observed, while

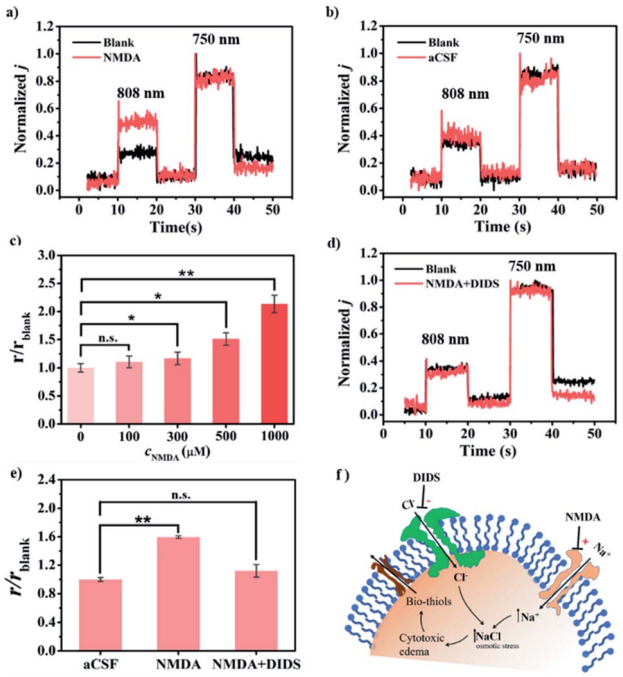

Fig. 5 Normalized photocurrent intensities of **CyOThiols**/TiWE recorded in live rat brains pre- and post-local microinjection of (a) 500 μM NMDA (1 μL min^{-1} for 60 s, $n = 3$) and (b) aCSF (1 μL min^{-1} for 60 s, $n = 3$). (c) Concentration-dependence of NMDA on the r/r_{Blank} values, where r_{Blank} is the value of j_{808}/j_{750} obtained before microinjection and r is that obtained after microinjection. (d) Normalized photocurrent intensities of **CyOThiols**/TiWE in rat brains before and after co-injection with 500 μM NMDA and 5 mM DIDS (1 μL min^{-1} for 60 s, $n = 3$). (e) The r/r_{Blank} values of aCSF (1 μL min^{-1} for 60 s, $n = 3$), 500 μM NMDA (1 μL min^{-1} for 60 s, $n = 3$), and co-injection of 500 μM NMDA and 5 mM DIDS (1 μL min^{-1} for 60 s, $n = 3$). (f) Schematic illustration of the possible mechanism of thiol efflux during cytotoxic edema. Data are mean ± standard deviation; $*p < 0.05$ and $**p < 0.01$, compared with control.

the fluorescence enhancement can be efficiently inhibited by DIDS. These results of *in vivo* imaging further proved the mercaptan release during cytotoxic edema. Interestingly, previous studies had elaborately demonstrated that NMDA activation could induce organic anion (*e.g.* ascorbate) release by inducing uncharted organic anion channel opening.[21] In this regard, our finding of cytotoxic edema-dependent thiol efflux may have offered an additional possible mechanism to understand this complicated physiological and pathophysiological molecular event (Fig. 5f).

Defining the sensibility of analytes in different brain regions will help to better understand the potential mechanism underlying physiological or pathological events. Here, the as-constructed microsensor was employed to detect the changes of thiols in different brain regions of kainic acid (KA)-induced epilepsy in rat brains.[22] Fig. 6a and b show the representative normalized photocurrent intensities in the hippocampi and cortexes of three groups (control group, KA II group and KA III group). In comparison to the control group, the r value obtained in the hippocampus was reduced to 82.2% and 55.7% as symptoms of epileptogenesis increased to the Racine II stage

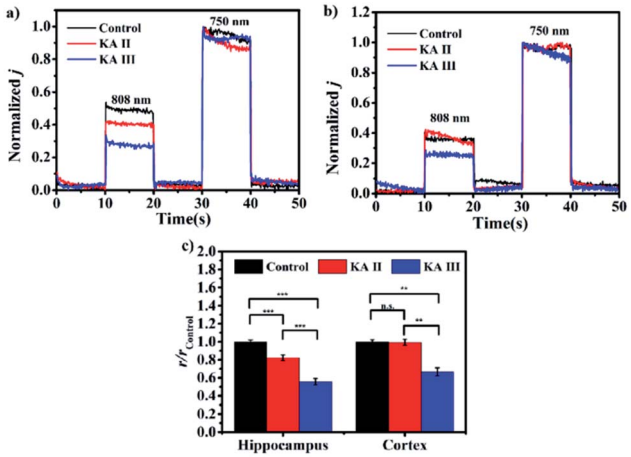

Fig. 6 Normalized photocurrent intensities of **CyOThiols**/TiWE recorded in the hippocampus (a) and cortex (b) of three groups: control group (saline), KA II group (30 mg kg^{-1} KA to induce Racine II stage epilepsy) and KA III group (50 mg kg^{-1} KA to induce Racine III stage epilepsy). (c) The $r/r_{Control}$ values of the three groups corresponding to (a) and (b) ($n = 3$). Data are mean ± standard deviation; $^{**}p < 0.01$ and $^{***}p < 0.001$.

and Racine III stage, respectively, suggesting the depletion of thiols with the progress of epileptogenesis. For the cortex, the *r* value was reduced to 99.4% and 66.6% in the two stages. It is worth noting that the decreasing degree of the observed *r* value in the hippocampus was significantly greater than that in the cortex, which may suggest higher sensitivity to epilepsy in the hippocampus region. Previous studies revealed a close crosstalk between the oxidative stress and epilepsy and showed that an increase in the levels of oxidizing substances (reactive oxygen, reactive nitrogen and active chlorine) is associated with epilepsy. Hence, the observed reduction in thiol concentration may result from thiol consumption caused by oxidative stress.[23]

Conclusions

In summary, we have proposed a strategy for constructing a near-infrared light driven ratiometric PEC microsensor based on a small-molecule organic semiconductor. Taking advantage of small molecules, *i.e.*, the high flexibility of the molecular structure and easily adjustable energy gap, the optical absorption of **CyOH** can be modulated by substituting different groups at the –OH position *via* an ICT process. By embedding a specific recognition site on–OH, a proof-of-concept probe, **CyOThiols**, was prepared and covalently bonded to the surface of TiWE to fabricate a microsensor for thiols. The highly specific reaction with thiols caused a red shift of **CyOThiols** absorption from 734 nm to 795 nm. Under excitation of two monochromatic lasers (808 nm and 750 nm), the microsensor yielded ratiometric photocurrent responses towards thiols, which exhibited good anti-interfering capacity owing to the self-calibration ability of the ratiometric signals. The **CyOThiols**/TiWE microsensor was applied to monitor thiol fluctuation in rat brains with a model of cerebral edema, which revealed that the NMDA-induced astrocyte swelling resulted in enhanced thiol release. Furthermore, it was utilized to monitor thiols in two regions of rat brains with KA-induced epilepsy. The variation of thiol concentration in the hippocampus differed from that in the cortex, suggesting higher sensitivity to epilepsy in the hippocampus region. The SMOS-based ratiometric PEC sensor resolved the problem of specificity and reliability of PEC sensing *in vivo*, and moreover, this strategy can be readily extended to diverse analytes by simply changing the recognition site of the probe.

Ethical statement

All animal studies were performed according to the Guidelines for the Care and Use of Laboratory Animals of the Chinese Animal Welfare Committee and approved by the Institutional Animal Care and Use Committee, Wuhan University Center for Animal Experiment, Wuhan, China.

Data availability

Additional data is available in the ESI.†

Author contributions

Y. Xiang and Y. Kong: most of the experiments and writing of the manuscript. W. Feng: DFT calculations and writing of the Theoretical calculations section. X. Ye: supervision of experiments, discussion, and writing of the manuscript. Z. Liu: conceptualization, funding acquisition, and supervision; writing, review, and editing of the manuscript.

Conflicts of interest

There are no conflicts to declare.

Acknowledgements

This work was supported by the National Natural Science Foundation of China (No. 21906047 and 21625503) and Natural Science Fund for Creative Research Groups of Hubei Province of China (2020CFA035).

References

1 (*a*) D. L. Robinson, A. Hermans, A. T. Seipel and R. M. Wightman, *Chem. Rev.*, 2008, **108**, 2554–2584; (*b*) H. Hou, Y. Jin, H. Wei, W. Ji, Y. Xue, J. Hu, M. Zhang, Y. Jiang and L. Mao, *Angew. Chem., Int. Ed.*, 2020, **59**, 18996–19000; (*c*) M. Spanos, X. Xie, J. Gras-Najjar, S. C. White and L. A. Sombers, *ACS Chem. Neurosci.*, 2019, **10**, 1497–1505; (*d*) X. Li, L. Ren, J. Dunevall, D. Ye, H. S. White, M. A. Edwards and A. G. Ewing, *ACS Nano*, 2018, **12**, 3010–3019; (*e*) C. J. Meunier and L. A. Sombers, in *The Brain Reward System*, ed. M. Fakhoury, Springer US, New York, NY, 2021, pp. 93–123.

2 (*a*) C. N. Hobbs, G. Holzberg, A. S. Min and R. M. Wightman, *ACS Chem. Neurosci.*, 2017, **8**, 2512–2521; (*b*) N. T. Rodeberg, S. G. Sandberg, J. A. Johnson, P. E. Phillips and R. M. Wightman, *ACS Chem. Neurosci.*, 2017, **8**, 221–234; (*c*) L. R. Walton, N. G. Boustead, S. Carroll and R. M. Wightman, *ACS Chem. Neurosci.*, 2017, **8**, 1598–1608; (*d*) C. Zhang, Z. Liu, L. Zhang, A. Zhu, F. Liao, J. Wan, J. Zhou and Y. Tian, *Angew. Chem., Int. Ed.*, 2020, **59**, 20499–20507; (*e*) F. Zhao, Y. Liu, H. Dong, S. Feng, G. Shi, L. Lin and Y. Tian, *Angew. Chem., Int. Ed.*, 2020, **59**, 10426–10430; (*f*) A. A. Gomez, T. A. Shnitko, H. M. Barefoot, E. L. Brightbill, L. A. Sombers, S. M. Nicola and D. L. Robinson, *ACS Chem. Neurosci.*, 2019, **10**, 1935–1940.

3 (*a*) J. Shu and D. Tang, *Anal. Chem.*, 2020, **92**, 363–377; (*b*) Y. Long, C. Kong, D. Li, Y. Li, S. Chowdhury and H. Tian, *Small*, 2011, **7**, 1624–1628; (*c*) L. Guo, Z. Li, K. Marcus, S. Navarro, K. Liang, L. Zhou, P. D. Mani, S. J. Florczyk, K. R. Coffey, N. Orlovskaya, Y. H. Sohn and Y. Yang, *ACS Sens.*, 2017, **2**, 621–625; (*d*) A. Ikeda, M. Nakasu, S. Ogasawara, H. Nakanishi, M. Nakamura and J. Kikuchi, *Org. Lett.*, 2009, **11**, 1163–1166.

4 W. W. Zhao, J. J. Xu and H. Y. Chen, *Chem. Rev.*, 2014, **114**, 7421–7441.

5 B. Fu and Z. Zhang, *Nano Lett.*, 2019, **19**, 9069–9074.

6 Z. Liu, X. Ye, X. Wang, Y. Kong, M. Dai and D. Han, *Angew. Chem., Int. Ed.*, 2021, **60**, 11774–11778.

7 H. Jin, Z. Sun, Y. Sun and R. Gui, *TrAC, Trends Anal. Chem.*, 2021, **134**, 116–124.

8 L. Wu, C. Huang, B. P. Emery, A. C. Sedgwick, S. D. Bull, X.-P. He, H. Tian, J. Yoon, J. L. Sessler and T. D. James, *Chem. Soc. Rev.*, 2020, **49**, 5110–5139.

9 (*a*) Q. Hao, X. Shan, J. Lei, Y. Zang, Q. Yang and H. Ju, *Chem. Sci.*, 2016, **7**, 774–780; (*b*) Z. Qiu, J. Shu, J. Liu and D. Tang, *Anal. Chem.*, 2019, **91**, 1260–1268.

10 H. Wu, H. L. Tan, C. Y. Toe, J. Scott, L. Wang, R. Amal and Y. H. Ng, *Adv. Mater.*, 2020, **32**, e1904717.

11 J. M. Cole, G. Pepe, O. K. Al Bahri and C. B. Cooper, *Chem. Rev.*, 2019, **119**, 7279–7327.

12 (*a*) L. Yuan, W. Lin, S. Zhao, W. Gao, B. Chen, L. He and S. Zhu, *J. Am. Chem. Soc.*, 2012, **134**, 13510–13523; (*b*) J. Li and K. Pu, *Chem. Soc. Rev.*, 2019, **48**, 38–71.

13 The pK_a was calculated according to the Henderson–Hasselbalch-type mass action equation $(\log[(F_{max} - F)/(F - F_{min})] = pK_a - pH)$ at 780 nm.

14 T. Lu and F. Chen, *J. Comput. Chem.*, 2012, **33**, 580–592.

15 A. Gómez-A, T. A. Shnitko, H. M. Barefoot, E. L. Brightbill, L. A. Sombers, S. M. Nicola and D. L. Robinson, *ACS Chem. Neurosci.*, 2019, **10**, 1935–1940.

16 J. A. Cooper, M. Wu and R. G. Compton, *Anal. Chem.*, 1998, **70**, 2922–2927.

17 (*a*) J. D. Majmudar, A. M. Konopko, K. J. Labby, C. T. M. B. Tom, J. E. Crellin, A. Prakash and B. R. Martin, *J. Am. Chem. Soc.*, 2016, **138**, 1852–1859; (*b*) S. Seshadri, A. Beiser, J. Selhub, P. F. Jacques, I. H. Rosenberg, R. B. D'Agostino, P. W. F. Wilson and P. A. Wolf, *N. Engl. J. Med.*, 2002, **346**, 476–483; (*c*) Y. Shi and K. S. Carroll, *Acc. Chem. Res.*, 2020, **53**, 20–31; (*d*) K. Umezawa, M. Yoshida, M. Kamiya, T. Yamasoba and Y. Urano, *Nat. Chem.*, 2016, **9**, 279–286.

18 (*a*) J. Sabate Del Rio, O. Y. F. Henry, P. Jolly and D. E. Ingber, *Nat. Nanotechnol.*, 2019, **14**, 1143–1149; (*b*) Y. Zhang, N. Hao, Z. Zhou, R. Hua, J. Qian, Q. Liu, H. Li and K. Wang, *Chem. Commun.*, 2017, **53**, 5810–5813.

19 (*a*) A. V. Molofsky, R. Krencik, E. M. Ullian, H. H. Tsai, B. Deneen, W. D. Richardson, B. A. Barres and D. H. Rowitch, *Genes Dev.*, 2012, **26**, 891–907; (*b*) L. E. Clarke and B. A. Barres, *Nat. Rev. Neurosci.*, 2013, **14**, 311–321; (*c*) I. D. Vainchtein, G. Chin, F. S. Cho, K. W. Kelley, J. G. Miller, E. C. Chien, S. A. Liddelow, P. T. Nguyen, H. Nakao-Inoue, L. C. Dorman, O. Akil, S. Joshita, B. A. Barres, J. T. Paz, A. B. Molofsky and A. V. Molofsky, *Science*, 2018, **359**, 1269–1273; (*d*) S. Sheikhbahaei, E. A. Turovsky, P. S. Hosford, A. Hadjihambi, S. M. Theparambil, B. Liu, N. Marina, A. G. Teschemacher, S. Kasparov, J. C. Smith and A. V. Gourine, *Nat. Commun.*, 2018, **9**, 370; (*e*) H. Mestre, T. Du, A. M. Sweeney, G. Liu, A. J. Samson, W. Peng, K. N. Mortensen, F. F. Staeger, P. A. R. Bork, L. Bashford, E. R. Toro, J. Tithof, D. H. Kelley, J. H. Thomas, P. G. Hjorth, E. A. Martens, R. I. Mehta, O. Solis, P. Blinder, D. Kleinfeld, H. Hirase, Y. Mori and M. Nedergaard, *Science*, 2020, **367**, 1211–1226; (*f*) J. A. Stogsdill, J. Ramirez, D. Liu, Y. H. Kim, K. T. Baldwin, E. Enustun, T. Ejikeme, R.-R. Ji and C. Eroglu, *Nature*, 2017, **551**, 192–197.

20 (*a*) J. Glykys, V. Dzhala, K. Egawa, K. T. Kahle, E. Delpire and K. Staley, *Trends Neurosci.*, 2017, **40**, 276–294; (*b*) R. L. Rungta, H. B. Choi, J. R. Tyson, A. Malik, L. Dissing-Olesen, P. J. C. Lin, S. M. Cain, P. R. Cullis, T. P. Snutch and B. A. MacVicar, *Cell*, 2015, **161**, 610–621; (*c*) P. Rivetti di Val Cervo, R. A. Romanov, G. Spigolon, D. Masini, E. Martín-Montañez, E. M. Toledo, G. La Manno, M. Feyder, C. Pifl, Y.-H. Ng, S. P. Sánchez, S. Linnarsson, M. Wernig, T. Harkany, G. Fisone and E. Arenas, *Nat. Biotechnol.*, 2017, **35**, 444–452.

21 J. Jin, W. Ji, L. Li, G. Zhao, W. Wu, H. Wei, F. Ma, Y. Jiang and L. Mao, *J. Am. Chem. Soc.*, 2020, **142**, 19012–19016.

22 R. J. Racine, *Electroencephalogr. Clin. Neurophysiol.*, 1975, **38**, 1–12.

23 K. R. N. Gibson, I. L. Neilson, F. Barrett, T. J. Winterburn, S. Sushma, S. M. MacRury and L. L. Megson, *J. Cardiovasc. Pharmacol.*, 2009, **54**, 319–326.